

Crustal structure of the Transantarctic Mountains near the Ross Sea from ambient seismic noise tomography

Moira L. Pyle,^{1,2} Douglas A. Wiens,¹ Andrew A. Nyblade,³ and Sridhar Anandakrishnan³

Received 28 October 2009; revised 1 February 2010; accepted 24 May 2010; published 11 November 2010.

[1] We derive a model for crustal shear wave velocities in the Transantarctic Mountains and surrounding areas of East Antarctica and the Ross Sea region of West Antarctica using Rayleigh wave Green's functions estimated from the cross correlation of ambient seismic noise recorded by the Transantarctic Mountains Seismic Experiment. Group velocity maps are determined from travel times measured from the Rayleigh waves filtered at periods between 5 and 23 s. The velocity maps are inverted for shear velocities across the region using a niching genetic algorithm. We observe only minor variation in crustal velocities beneath East Antarctica and the Transantarctic Mountains, and velocities are similar to those observed for Precambrian crust worldwide. Low velocities, which may be related to the presence of sediment, are observed at shallow depths beneath the Wilkes Subglacial Basin and the Aurora Subglacial Basin, but dispersion curves show that sediment thickness must be limited to less than about 2 km. In the Ross Sea, we observe low velocities at shallow depths from thick sediments and high velocities approaching mantle values between 16 and 20 km depth.

Citation: Pyle, M. L., D. A. Wiens, A. A. Nyblade, and S. Anandakrishnan (2010), Crustal structure of the Transantarctic Mountains near the Ross Sea from ambient seismic noise tomography, *J. Geophys. Res.*, *115*, B11310, doi:10.1029/2009JB007081.

1. Introduction

[2] The extensive ice coverage of Antarctica creates a challenging environment in which to study the subglacial structure of the continent. Direct observations are limited to the few rock outcrops located mostly near the coastline, and geophysical studies are expensive and logistically difficult to carry out. The result of these difficulties is a poorly constrained knowledge of the geological history and structure. Improving our knowledge of crustal seismic velocities allows for better determination of crustal thicknesses and is important for constraining geological and geodynamical models. Additionally, better knowledge of shallow crustal structure, in particular the location of sediment, may contribute to advancing our understanding of glacial movement and how it is influenced by the subglacial geology [Anandakrishnan *et al.*, 1998; Anandakrishnan and Winberry, 2004; Bell *et al.*, 1998; DeConto and Pollard, 2003; Donda *et al.*, 2007; Escutia *et al.*, 2005].

[3] An area of particular interest in Antarctica is the region of the Transantarctic Mountains (TAMs) near the Ross Sea (RS) and adjoining areas in East Antarctica (EA)

and the West Antarctica Rift System (Figure 1). The Transantarctic Mountains are a 4000 km long mountain range, marking the boundary between East and West Antarctica, which lack evidence of a compressional tectonic origin. Crustal thicknesses found beneath the TAMs are mostly on the order of 35–40 km [e.g., Bannister *et al.*, 2003; Della Vedova *et al.*, 1997; Lawrence *et al.*, 2006a, 2006b; O'Connell and Stepp, 1993]. East Antarctica is believed to be a Precambrian craton, which formed a large portion of the supercontinent Gondwana [Dalziel, 1992]. Estimates of crustal thickness from surface waves and receiver function analysis range from about 35 to 45 km [Hansen *et al.*, 2009; Lawrence *et al.*, 2006a, 2006b; Ritzwoller *et al.*, 2001]. West Antarctica is a younger amalgamation of distinct terranes, characterized by extension and volcanism during the Cenozoic [Behrendt *et al.*, 1991]. The rifting extends beneath the Ross Sea, which has been extensively studied by active source seismic surveys. Most of these studies find crustal thicknesses ranging from 17 to 28 km [e.g., Behrendt, 1999; Bentley, 1991; Cooper *et al.*, 1987; Della Vedova *et al.*, 1997]. A major question for this region concerns the geodynamic models for the uplift of the TAMs. There is considerable debate about the tectonic mechanism of the TAMs uplift and its relationship to the rifting and volcanism in West Antarctica as well as topographical features such as the Wilkes Subglacial Basin in EA [e.g., Lawrence *et al.*, 2006a; Studinger *et al.*, 2004; ten Brink *et al.*, 1993, 1997].

[4] Many previous studies have sought to image the crust and mantle structure in and around this area through conti-

¹Department of Earth and Planetary Sciences, Washington University in St. Louis, St. Louis, Missouri, USA.

²Now at Department of Geology and Geophysics, University of Utah, Salt Lake City, Utah, USA.

³Department of Geosciences, Pennsylvania State University, University Park, Pennsylvania, USA.

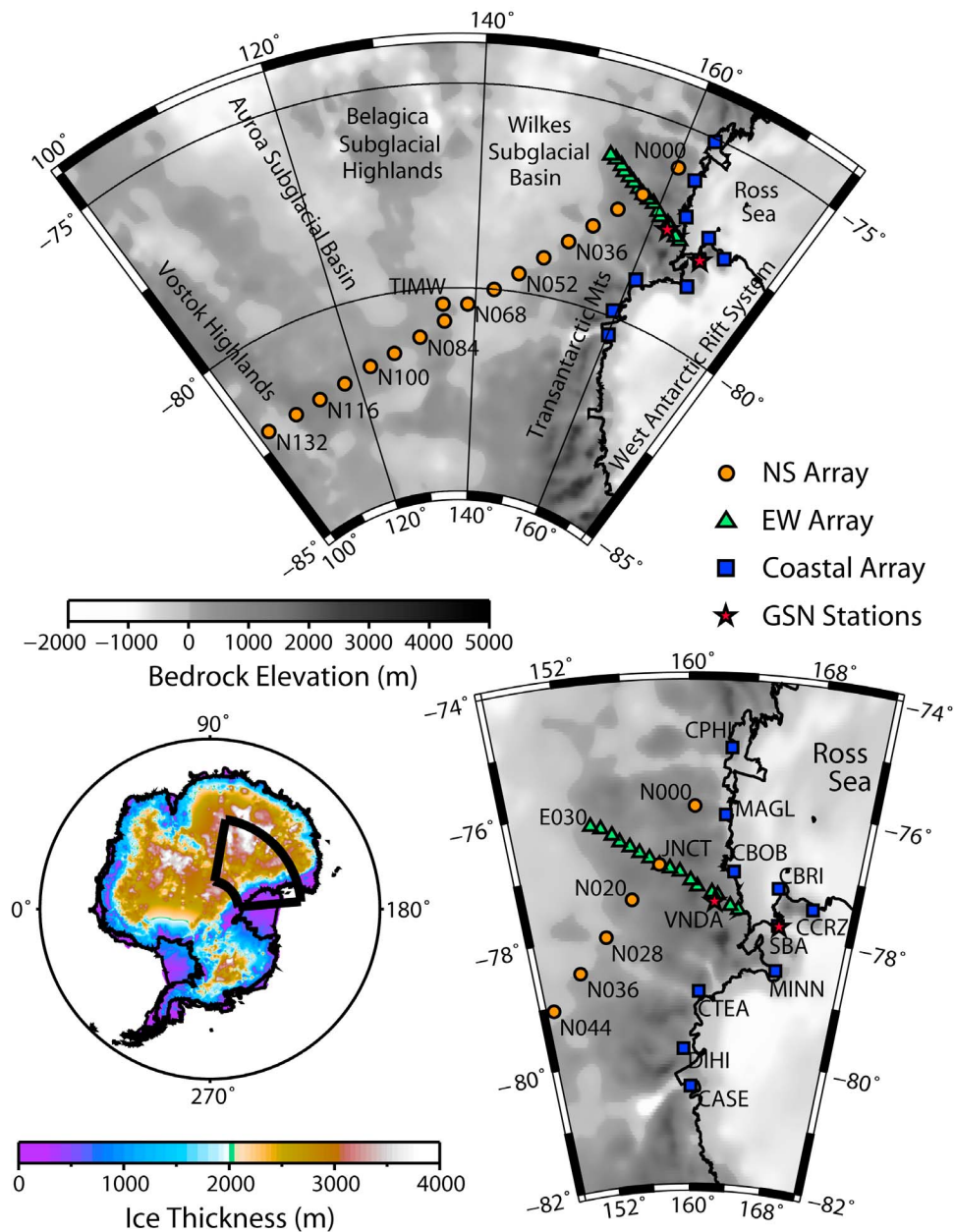


Figure 1. Map of TAMSEIS stations. Symbols denote stations in different subarrays: (orange) circles indicate stations in the north–south subarray, (green) triangles indicate stations in the east–west subarray, (blue) squares indicate stations in the coastal subarray, and (red) stars denote permanent GSN stations. Background shading represents the subglacial bedrock elevation. Some station names and names of subglacial features are indicated on the map. Bottom left shows the location of the TAMSEIS array with respect to the Antarctic continent. Shading in the continental map indicates ice thicknesses from BEDMAP [Lythe *et al.*, 2001]. Bottom right shows a close up of coastal and east–west subarray stations.

mental scale surface wave studies [e.g., Morelli and Danesi, 2004; Ritzwoller *et al.*, 2001; Roult *et al.*, 1994], local receiver functions [Anandakrishnan and Winberry, 2004; Bannister *et al.*, 2003; Kanao *et al.*, 2002], and gravity and magnetic studies [Studinger *et al.*, 2004]. Recently, the region has been studied in detail using data from the Transantarctic Mountain Seismic Experiment (TAMSEIS), the first large-scale broadband seismic deployment in Antarctica [Lawrence *et al.*, 2006a, 2006b; Watson *et al.*, 2006].

Results from this experiment have provided a much more detailed picture of the crustal thickness and upper mantle seismic velocity than was previously possible. However, for the most part, the previous studies have provided only limited resolution of the structure within the crust. Potential field methods, such as gravity and magnetics, are inherently nonunique, and seismic receiver function studies are subject to a tradeoff between crustal velocities and crustal thickness. Seismic surface waves provide some constraints on crustal

structure but are limited in shallow resolution since the periods usable in traditional studies are mostly sensitive to mantle depths.

[5] Recent advances in acoustics and seismology have led to the development of a new seismic imaging method known as ambient noise correlation. This method retrieves the interstation Green's function by correlating diffuse wavefields at two different seismic stations. It is particularly useful for examining crustal structure since the excitation of noise predominately occurs at short periods allowing for the determination of accurate surface wave velocities at periods of less than 25 s without many of the difficulties associated with surface wave propagation from earthquakes at these periods. The noise correlation technique is based on the premise that cross-correlating diffuse waves between two points will generate the Green's function between those points [e.g., *Derode et al.*, 2003; *Lobkis and Weaver*, 2001]. Sufficient randomization of the seismic noise to produce a diffuse wavefield is thought to be obtained from considering long time periods of recorded data (generally anywhere from 1 month to 1 year) [*Sabra et al.*, 2005a; *Shapiro and Campillo*, 2004] or by using coda waves from many earthquakes [*Campillo and Paul*, 2003; *Paul et al.*, 2005]. Many studies have demonstrated that correlograms obtained from the cross correlation of long time series of vertical component ambient seismic noise can be filtered at various periods to obtain dispersion curves, which can be used to generate group velocity maps and perform surface wave tomography [e.g., *Bensen et al.*, 2007; *Sabra et al.*, 2005b; *Shapiro et al.*, 2005; *Yang et al.*, 2007].

[6] In this paper, we use the noise correlation method and data from the TAMSEIS experiment to develop a model of the crustal seismic velocities beneath a portion of the TAMs, EA, and the RS. Very little information about the detailed crustal structure in this region was previously available. Additionally, we investigate the possibility of the presence of sediment within the Wilkes Subglacial Basin.

2. Data

[7] The Transantarctic Mountain Seismic Experiment (TAMSEIS) consisted of 42 temporary broadband seismic stations installed between the Ross Sea and the Vostok highlands (Figure 1). This project was a large-scale broadband seismometer deployment located in Antarctica and was designed to examine the transition between the East Antarctic highlands and the West Antarctic Rift System along the Transantarctic Mountains. The experiment ran from December 2000 until December 2003 with seismometers using batteries and solar power to run during the austral summer. The stations shut down due to lack of power during the winter months and in many cases restarted when the sun came up. All stations consisted of a broadband seismograph (in most cases a Guralp CMG-3T) and a 24 bit datalogger (Reftek 72A-08) with GPS timing.

[8] Eight of the stations were installed in December 2000, while the remaining 34 stations were deployed in November and December of 2001. The array of stations can be divided into three subarrays: a coastal array of 9 stations with a roughly N–S orientation along the mainland coastline and Ross Island, an array striking roughly E–W of 16 stations with about 20 km spacing, and an array striking roughly

NNE–SSW of 17 stations (station JNCT is shared with the E–W subarray) with about 80 km spacing. The coastal array stations and the EW array stations from E000 to E010 were installed at rock sites, whereas the rest of the EW array stations and all the NS array stations with the exception of N000 were installed on top of the ice sheet. In addition to the TAMSEIS stations, we also use data from two permanent Global Seismographic Network stations, Vanda (VNDA) and Scott Base (SBA). Coordinates of all stations are given in the work of *Lawrence et al.* [2006b].

[9] Most TAMSEIS stations operated well during the months of November to March providing up to a total of 12 months of data for the main deployment. However, due to the difficulty of running seismic stations in such extreme conditions, many stations experienced periods of downtime, so the resulting availability of data varies considerably from station to station, and correlating a station pair obviously requires that both stations be operating simultaneously. Three stations, E022, N052, and CCRZ, returned very limited data with insufficient time duration to obtain good Green's functions by correlation with other stations. On average, we found that we were able to correlate between 3 and 4 months of data for station pairs with the remaining TAMSEIS and GSN stations.

3. Methods and Results

3.1. Noise Correlation

[10] We use vertical component data to examine the Rayleigh wave portion of the estimated Green's functions, generally following the data processing procedure of *Bensen et al.* [2007]. Data are processed in day-long segments, and for each station pair, we require that for a day to be included both stations must have at least 23 h of continuous data recorded. We use data from the 40 sample/s data stream and decimate all time series to 5 samples/s. For each day-long time series, we first remove the instrument response, demean and detrend the data, and apply a bandpass filter between 3 and 80 s. Next we remove the effect of any earthquakes which might dominate the correlation by normalizing the time series with a running absolute mean. This method of normalization calculates the average value of the absolute value of the waveform amplitude in a moving, 50 s long window. The center point of each window is inversely weighted by the average. Finally, each trace is spectrally whitened.

[11] For each pair of stations, we cross-correlate each day-long segment in the frequency domain and then stack all the day-long correlograms in the time domain. After stacking the data, we average the positive and negative lags of the correlogram to find the "symmetric component." If the recorded noise wavefield were completely diffuse, the positive and negative lags would theoretically be identical, but in practice the noise has some directionality, and so the cross correlation is asymmetric. Averaging the two lags accounts for this heterogeneity in the noise wavefield [*Bensen et al.*, 2007]. We then use multiple filter analysis [*Dziewonski et al.*, 1969] where the estimated Green's function is filtered with a series of narrow-band filters in order to measure the group velocity at different periods.

[12] Several previous noise correlation studies have used seasonal variability in the correlograms to determine the

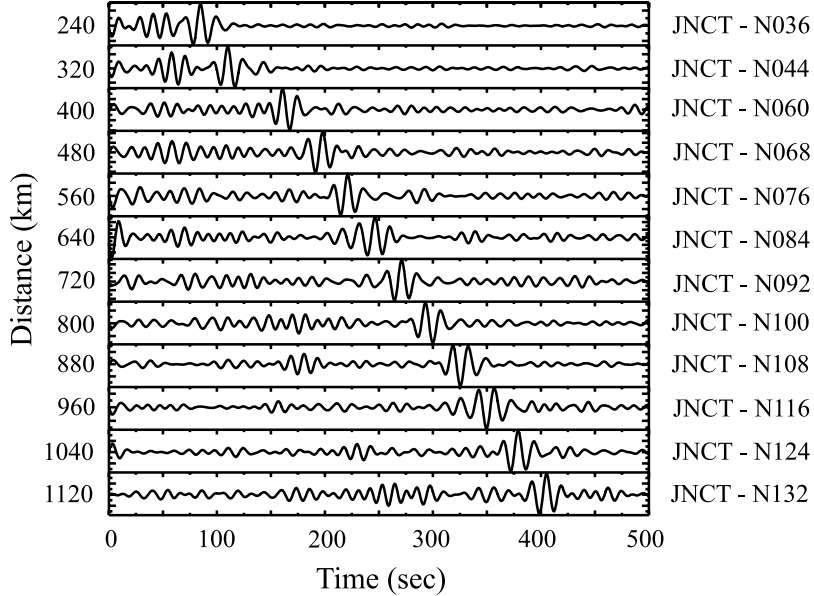


Figure 2. Example of symmetric component waveforms from the noise correlation method. Each correlation is between station JNCT (Figure 1) and each progressive station down the north–south subarray line of stations. Correlograms have been bandpass filtered between 10 and 20 s. All stations used in this figure are located on ice.

reliability of group velocity measurements [e.g., *Bensen et al.*, 2007, 2008; *Lin et al.*, 2007; *Yang et al.*, 2007]. Because we have data only from months during the austral summer, we are unable to perform a similar analysis. Instead, we use a bootstrap resampling method [*Efron and Tibshirani*, 1991] to identify station pairs that lack consistency in waveforms from day to day. For each station pair, 60 new stacks are created with randomly selected day-long segments. Velocities from each resampled stack are measured, and the standard deviation of the velocity measurements is calculated and used for quality control. We choose 60 stacks as a compromise between computation time and convergence of the results. Figure 2 shows an example of the resulting symmetric component correlograms. The top waveform is the correlation between station JNCT and station N036, the second waveform is between JNCT and N044, and so on down the NS line of stations (Figure 1). All of the stations in this example are located on ice. The moveout of the signal can be seen clearly.

[13] After all the correlograms have been calculated, we apply several selection criteria to eliminate poorly constrained Green's functions. First, we require a minimum of 40 days to be correlated in order to ensure stable velocity measurements. Second, in order to avoid cross contamination from the positive and negative lags from closely spaced stations, we require that the distance between stations be at least three wavelengths for the period being measured. Third, we eliminate data with a signal-to-noise ratio (SNR) of 7.0 or lower, where the SNR is defined as the highest amplitude in the window surrounding the waveform divided by the root mean square amplitude of the noise following the signal window. Fourth, we require that the bootstrap resampling method returns a standard deviation less than 0.1 km/s. After these automated criteria are applied, we still found it necessary to visually inspect all measurements and

discard those that had multiple and interfering peaks in the expected velocity window. Finally, we run the remaining data through an overly smoothed tomographic inversion and discard travel times that have residuals greater than 5% of the travel time residual from the average velocity. A total of 753 stations pairs were correlated making this number the maximum number of data available for any period. After the selection criteria are applied, approximately 68% of the pairs are usable at the best periods (8–12 s), while only about 39% of the pairs are usable at the worst periods (5, 26 s). Other studies see similar values of data retention with numbers as low as 33% for the worst periods [e.g., *Yang et al.*, 2007]. Figure 3 shows the interstation raypath coverage at select periods for paths which meet the selection criteria.

3.2. Surface Wave Tomography

[14] We perform a tomographic inversion of the group velocity measurements to obtain group velocity maps of the region at specific periods. We use a damped, smoothed, least squares method similar to that used for traditional surface wave phase velocity inversion by *Lawrence et al.* [2006b],

$$\begin{bmatrix} \Delta \vec{x} \\ \lambda \end{bmatrix} \begin{bmatrix} \vec{s} \end{bmatrix} = \begin{bmatrix} \Delta \vec{t} \\ 0 \end{bmatrix}, \quad (1)$$

where s is the slowness vector and λ is the first derivative smoothing constraint. The inversion is performed over a grid of 657 equally sized hexagonal blocks with half-degree spacing between nodes (block centers) (Figure 4), and each period is inverted separately. Nodes that are outside of the area with raypath coverage or have low resolution are discarded. We use a variable damping parameter, which is selected so that nodes with a high number of raypaths have a low amount of damping and nodes with a low density of

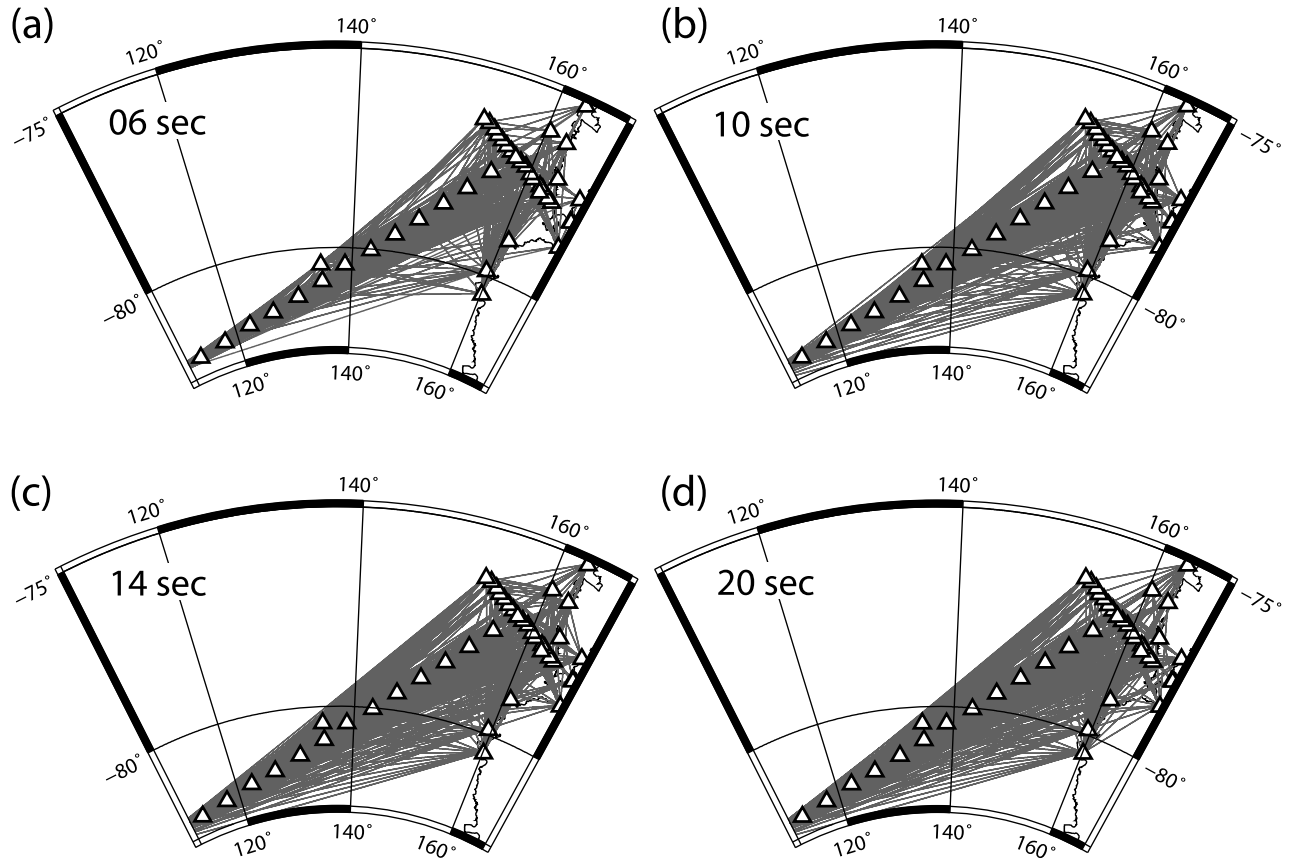


Figure 3. Interstation raypath coverage for (a) 6, (b) 10, (c) 14, and (d) 20 s periods. Only paths which meet the selection criteria described in the text are included.

raypaths are increasingly damped to the average value [Barmin et al., 2001]. The use of a constant damping parameter instead does not significantly change the results. We also tested a variety of smoothing parameters and chose a value which compromises the tradeoff between decreased variance and increased travel time residuals.

[15] We first invert for a single average group velocity for the entire region at each period. This result is shown in Figure 5a along with predicted group velocities from the crustal model for Archean age continental crust from CRUST 2.0 [Bassin et al., 2000]. The model is modified to include a 2 km thick ice layer with a V_s of 1.94 km/s, a 0.5 km thick sediment layer with a V_s of 2.10 km/s, and a 35 km thick crust to better represent average values for the TAMSEIS region. Our group velocity results show less variation than the model, increasing subtly from 2.93 km/s at 5 s to 2.97 km/s at 10 s and then decreasing very slightly to 2.95 km/s at 18 s and finally increasing again beyond 18 s to 2.98 km/s at 23 s. The differences in velocity compared to CRUST 2.0 range from about 0%–3%. We calculate errors by finding the L2 misfit between travel times predicted by the average value and travel times measured from each individual station pair. Errors are significant, but this is likely due to lateral heterogeneity. Error bars representing two standard deviations are plotted in Figure 9.

[16] To better examine the variable structures in our study area, we invert for regional averages in East Antarctica, the Transantarctic Mountains, and the Ross Sea. Nodes are

grouped into regions based on the tectonic structure as shown in Figure 4, and we use the uniform group velocities from Figure 5a as a starting model. The regional results are shown in Figure 5b. Errors, calculated for each region in the

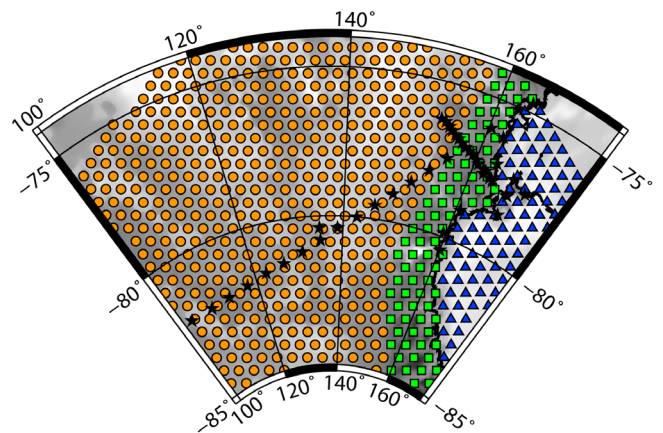


Figure 4. Nodes used in tomographic inversion. Each node represents the center of a hexagonal block. Dark gray (blue) triangles correspond to the Ross Sea region in West Antarctica, gray (green) squares correspond to the Transantarctic Mountains, and light gray (orange) circles correspond to the East Antarctica region. Black stars show seismic station locations.

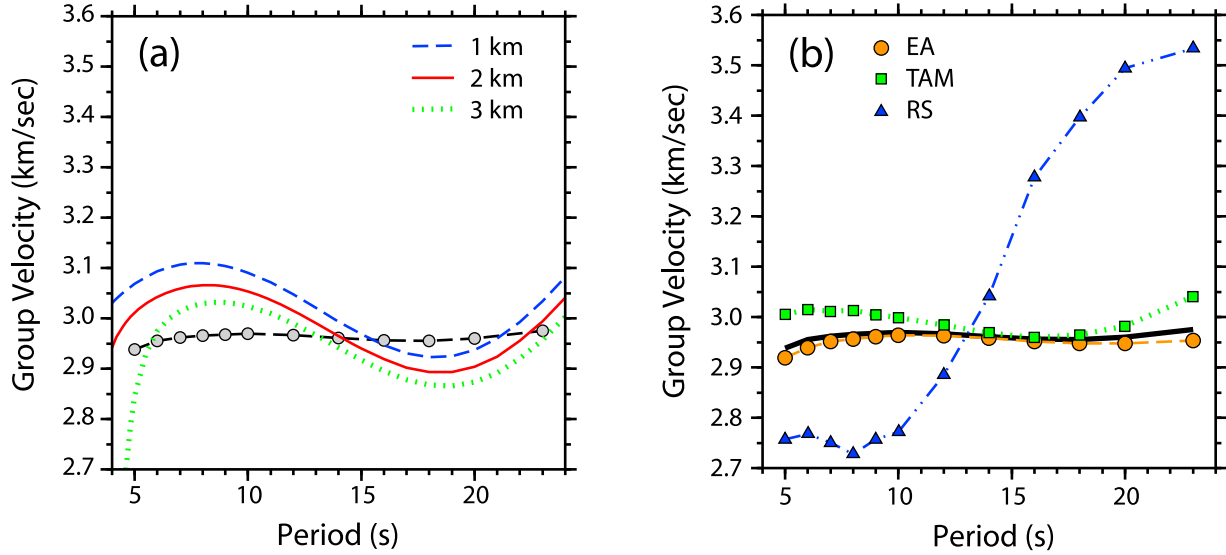


Figure 5. Average and regional group velocity curves. (a) The observed average group velocity curve is shown by gray circles. Solid black (red) line shows the group velocities predicted by the CRUST 2.0 model [Bassin et al., 2000] for Archean aged crust with a 2 km ice layer and a 35 km thick crust. Dark gray (blue) dashed and light gray (green) dotted lines show model with 1 and 3 km of ice, respectively. (b) Solid black line shows the average group velocity curve from Figure 5a and the regional curves are represented by dark gray (blue) triangles for the Ross Sea, gray (green) squares for the Transantarctic Mountains, and light gray (orange) circles for East Antarctica.

same way as for the average curve, are plotted in Figure 9. EA exhibits group velocities that are just slightly lower than the average velocities, varying by no more than 1% from the average. This suggests that the average velocity of the region is largely controlled by the velocity structure of EA. Velocities in the TAMs are higher than the average velocity curve at all periods with the greatest differences at the shortest and longest periods. At 5–6 s, the TAMs show velocities 2% higher than average. The difference decreases to ~0% at 16 s and then increases again to ~2% at 23 s. Group velocities in the RS are up to 6% lower than the average curve at short periods, decreasing slightly from 2.76 km/s at 6 s to 2.72 km/s at 8 s. At periods longer than 8 s, the velocities increase sharply, reaching 3.53 km/s at 23 s, which is ~16% higher than the average velocity.

[17] We next perform an inversion for laterally varying velocities using the average dispersion curve as a starting model. Group velocity maps for select periods are shown in Figure 6. Figure 7 shows resolution maps constructed from the diagonal elements of the model resolution matrix. The lowest velocities of 2.4–2.6 km/s lie beneath the RS and the Ross Ice Shelf at periods of 5–10 s. These velocities are up to 17% below the average velocity for the entire region and are probably attributable to thick sedimentation [e.g., Behrendt et al., 1991; Cooper et al., 1987; Kim et al., 1986]. At periods of 14 s and longer the RS and Ross Ice Shelf start showing velocities 11%–25% faster than the average due to the significantly thinner crust beneath the RS compared to the rest of the study area. The TAMs show velocities that are 9%–12% faster than average from 5 to 10 s. From 12 to 20 s, the velocities remain fairly consistently around the average, but beyond 20 s the velocities in the TAMs reach about 9% higher than average. In EA, low velocities of 2.4–2.6 km/s are observed beneath some portions of the Wilkes Sub-

glacial Basin at periods from 5 to 8 s. The area beneath the Belagica Subglacial Highlands exhibits higher than average velocities at all periods. Velocities are between 3% and 11% faster than average from 6 to 7 s, 1%–8% faster from 8 to 12 s, and 4%–10% faster for periods above 12 s. Some of the velocity differences at shorter periods can be attributed to varying ice thicknesses.

3.3. Shear Velocity Determination

[18] We invert our group velocities for best fitting shear velocity models using a niching genetic algorithm (NGA) [Koper et al., 1999; Lawrence and Wiens, 2004; Mafoud, 1995]. We briefly describe the method here, but more in-depth discussions on applying NGAs to seismic data can be found in the works of Koper et al. [1999] and Lawrence and Wiens [2004]. The NGA utilizes multiple populations to effectively search the model space. Initially, the models in each subpopulation are assigned parameters that are randomly generated within the supplied bounds. Each model is then evaluated by a cost function. Each subpopulation is forced to search a different portion of the model space by penalizing not only models that have a high cost due to poorly fitting the data, but also models which are too similar to models in higher-order populations. In each subpopulation, the model with the lowest cost is kept, and other models are combined and mutated for the next generation. The NGA searches for the shear velocity model which best minimizes a cost function described in equation (2),

$$\Sigma[2 \times V_{S_i} - V_{S_{i+1}} - V_{S_{i-1}}] \times \Sigma[\sigma^{-1} \times \text{abs}(U_{\text{obs}} - U_{\text{pred}})], \quad (2)$$

where V_{S_i} represents the shear velocity for the i th layer, U_{obs} and U_{pred} are the observed and predicted group velocities, respectively, and σ^{-1} represents the root mean square travel

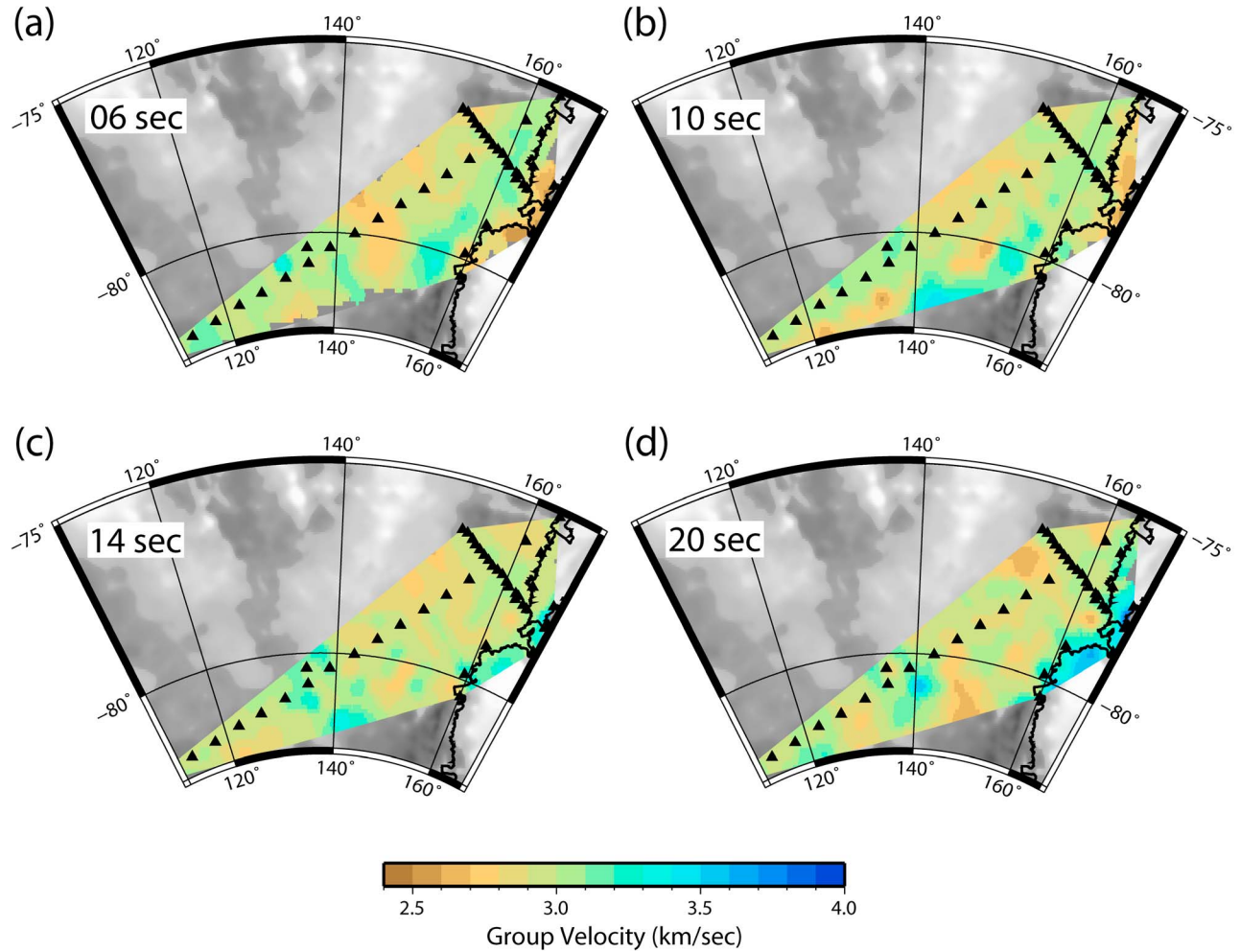


Figure 6. Group velocity maps for (a) 6, (b) 10, (c) 14, and (d) 20 s periods. Triangles show station locations. Bedrock topography is plotted in the background.

time misfits from the tomographic maps in Figure 6. The first half of the equation places a second derivative smoothing constraint on the shear velocity curve and the second half is the weighted L1 misfit between the observed group velocities and those predicted by the shear velocity model. The predicted group velocities are calculated using the work of *Herrmann* [1978].

[19] An advantage of the NGA is that it does not rely on an a priori starting model or predetermined layer thicknesses. We invert for layer thicknesses and shear wave velocities in five crustal layers. We include four layers which are allowed to vary between 1 and 8.5 km in thickness. The thickness of the fifth crustal layer is set to be equal to the sum of the thicknesses of layers one through four subtracted from the total crustal thickness. We use crustal thickness results from *Lawrence et al.* [2006a] for the study area average and TAMs region. For EA, we use crustal thicknesses from a recent receiver function study by *Hansen et al.* [2009]. For the RS, we allow crustal velocities to vary down to 26 km since the crust in the RS is believed to be significantly thinned and our group velocities should have sensitivity to the crustal thickness. The shear velocities are allowed to vary by $\pm 20\%$ of PREM [Dziewonski and Anderson, 1981] crustal velocities except for the upper-

most layer, which is allowed to search to lower velocities in the event that there might be sediment present. Velocities in the half-space beneath the five crustal layers are fixed at the upper mantle velocities found in the region from traditional phase velocity inversion by *Lawrence et al.* [2006b]. We also include a 2 km ice layer for the average and EA regional inversions. Rayleigh waves are only weakly sensitive to P wave velocities and densities, so we assume a P velocity model of $\sqrt{3}$ times the shear velocity model in each layer and determine the density from the velocity structure using the relationship of *Ravat et al.* [1999]. For each inversion, we run the NGA for 250 generations and include five populations with 20 models in each population adding up to a total search of 25,000 models.

[20] Shear velocity models calculated for the average and regional curves from Figure 5 are shown in Figure 8. In each case, the gray areas represent the range of models which have costs within 50% of the lowest cost model. Blue lines show the average of this range of models and red lines show the lowest cost model. The average and EA shear velocity models have a fixed 2 km ice layer and show similar structures with small increases in velocity from 2 to 20 km and a fairly constant velocity below ~ 20 km. Lower crustal velocities are comparable to those used for Archean crust in

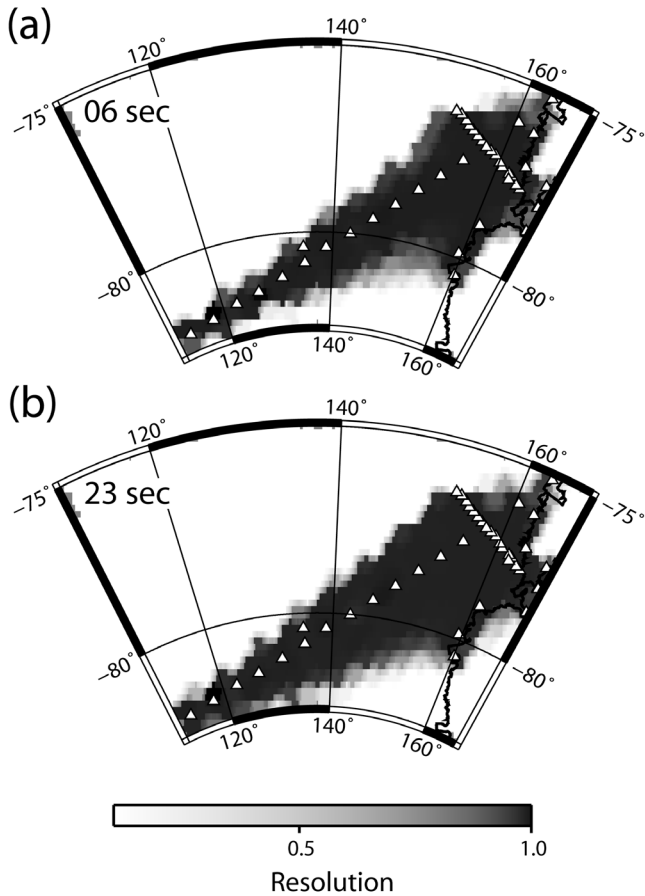


Figure 7. Resolution maps at (a) 6 and (b) 23 s periods. Maps are constructed from the diagonal elements of the model resolution matrix plotted at the corresponding geographical locations.

the CRUST 2.0 model [Bassin *et al.*, 2000], but shallow velocities are about 7% lower. The TAMs model also displays roughly the same trend as the average and EA models, with a slightly larger jump in velocity at 22 km depth. The RS region exhibits the lowest shear velocities of 3.2–3.3 km/s to

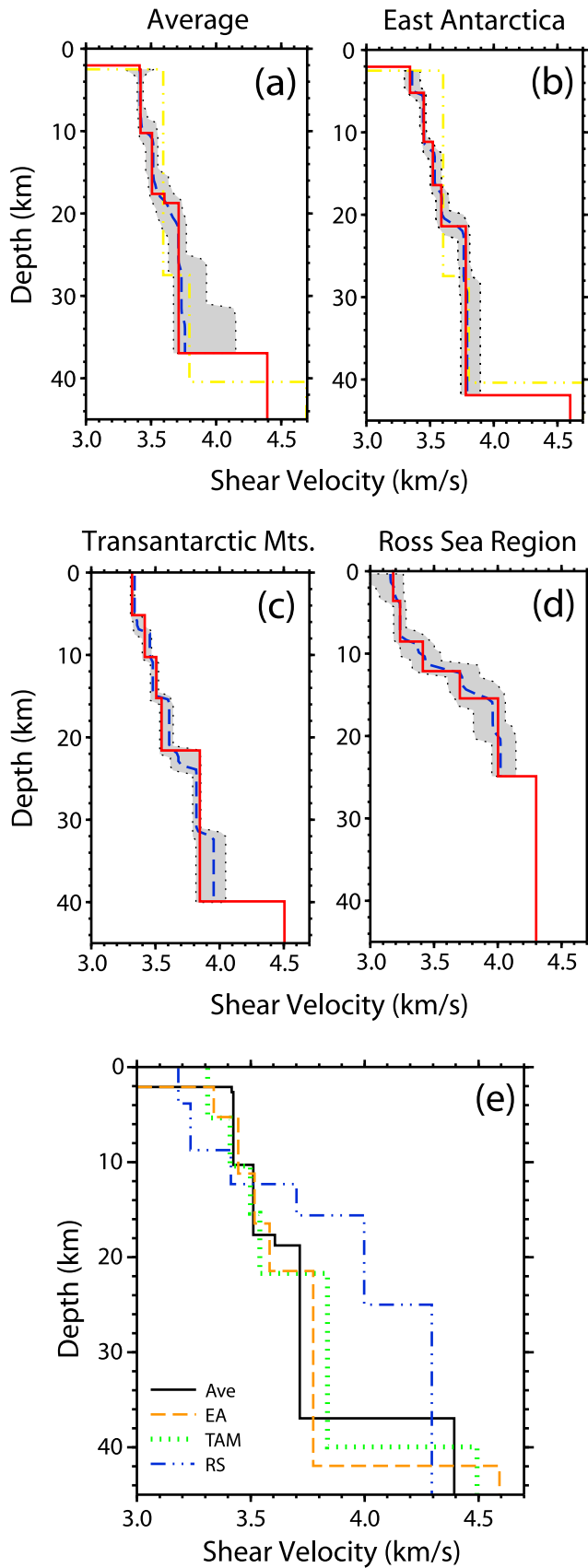


Figure 8. Average and regional shear velocity models determined from the inversion of group velocity curves in Figure 5. Models are for (a) the average, (b) East Antarctica, (c) the Transantarctic Mountains, and (d) the Ross Sea. In all cases, the best model, defined as the model with the lowest cost, is shown by the solid black (red) line. Gray areas correspond to the velocity and depth range spanned by models with costs within 50% of the best model. Dashed white (blue) line shows the average of models represented by the gray area. Gray (yellow) line in Figures 8a and 8b shows the CRUST 2.0 model [Bassin *et al.*, 2000] for Archean crust with a 2 km ice layer and a 0.5 km sedimentary layer. (e) Comparison of the best models in each case. Colors and line patterns are the same as in Figures 4 and 5: solid black for the average, light gray (orange) dashed for East Antarctica, gray (green) dotted for the Transantarctic Mountains, and dark gray (blue) dash-dotted for the Ross Sea.

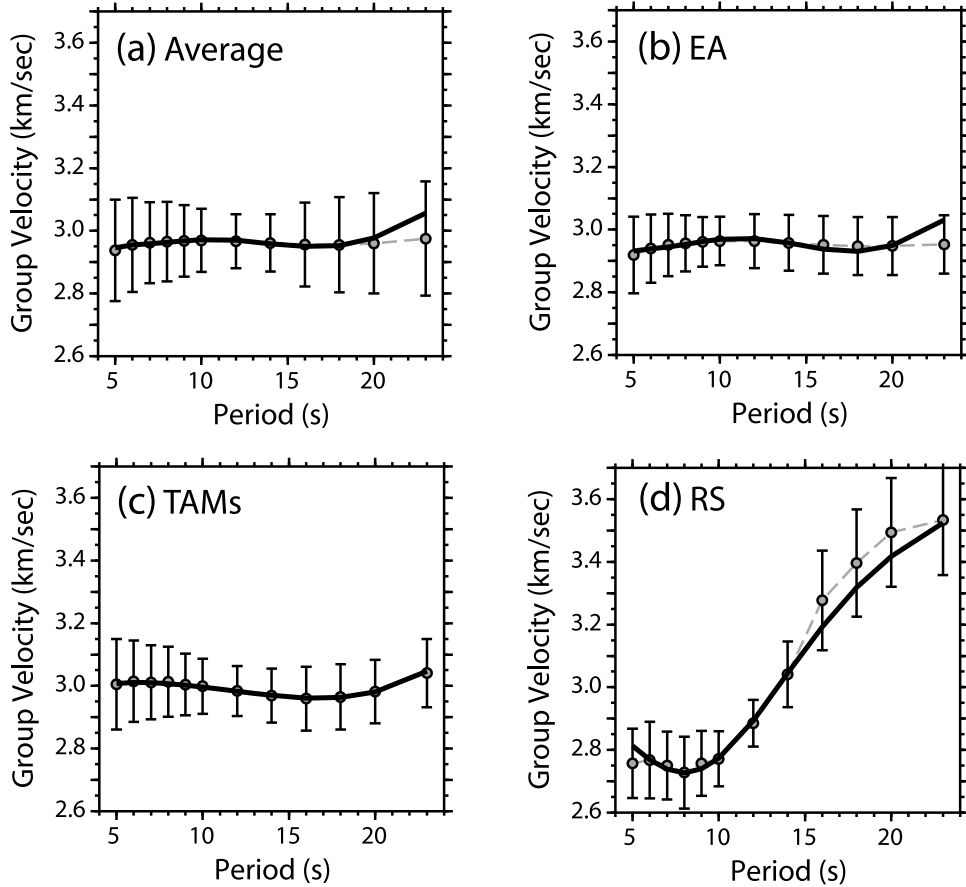


Figure 9. Fit to the data by shear velocity inversion results for (a) the average, (b) East Antarctica, (c) the Transantarctic Mountains, and (d) the Ross Sea. In all cases, gray circles show observed group velocities from Figure 5, and solid black lines show the predicted group velocities from the corresponding best shear velocity model shown in Figure 8.

~9 km depth. The velocity then increases steadily reaching a value of 4.0 km/s at about 16 km depth. Group velocities predicted from each of these shear velocity models and their corresponding observed group velocities (Figure 5) are shown in Figure 9. In all four cases, the fits are quite good.

[21] We construct shear velocity maps by inverting group velocities from the maps in Figure 6. At each inversion node, we use the group velocities from that node averaged with those from the immediately adjacent nodes and invert for shear velocity using the same method described above. Each point is assigned the crustal thickness and mantle velocity as described above for the region in which it falls. Ice thicknesses at each point are determined from the use of aerogeophysical data from the SOAR project [Blankenship *et al.*, 2001; Holt, 2001]. Where SOAR data are not available, we use ice thicknesses from BEDMAP [Lythe *et al.*, 2001]. Resulting shear velocity maps for selected depths are shown in Figure 10. Low velocities of ~3.2–3.3 km/s, 3%–6% lower than the average velocity, are observed at 4–8 km depth in the RS, at the edges of the Wilkes Subglacial Basin and in the vicinity of the Aurora Subglacial Basin. Velocities which are 3%–5% higher than average at 3.5–3.6 km/s are located beneath the TAMs and the Belagica Highlands. At about 12 km depth, velocities in the RS begin to show higher values of about 3.8–3.9 km/s at the edge of

the study area. This region of higher velocities increases in size and velocity as depth increases, reaching 4.3–4.5 km/s for the entire RS and Ice Shelf area by 22 km depth.

4. Discussion

4.1. The Ross Sea Region

[22] Previous surface wave investigations in Antarctica have been limited to mostly continental scale studies [e.g., Danesi and Morelli, 2001; Ritzwoller *et al.*, 2001] at longer periods with little resolution of crustal structure. A recent high-resolution Rayleigh wave study was conducted using data from the TAMSEIS deployment by Lawrence *et al.* [2006b], but due to limitations of traditional surface wave methods the shortest period examined by this study was 16 s which provides the only measurements of surface wave velocity which overlap with our study. The Lawrence *et al.* [2006b] study examined phase velocities while our study examines group velocities, and these two measurements have different sensitivity kernels, making it difficult to directly compare results. A crude comparison can be made by estimating phase velocities to have peak sensitivity to shear velocity structure at approximately 4/3 of the period while group velocities have peak sensitivity to a depth roughly equal to the period, and we do find similar veloci-

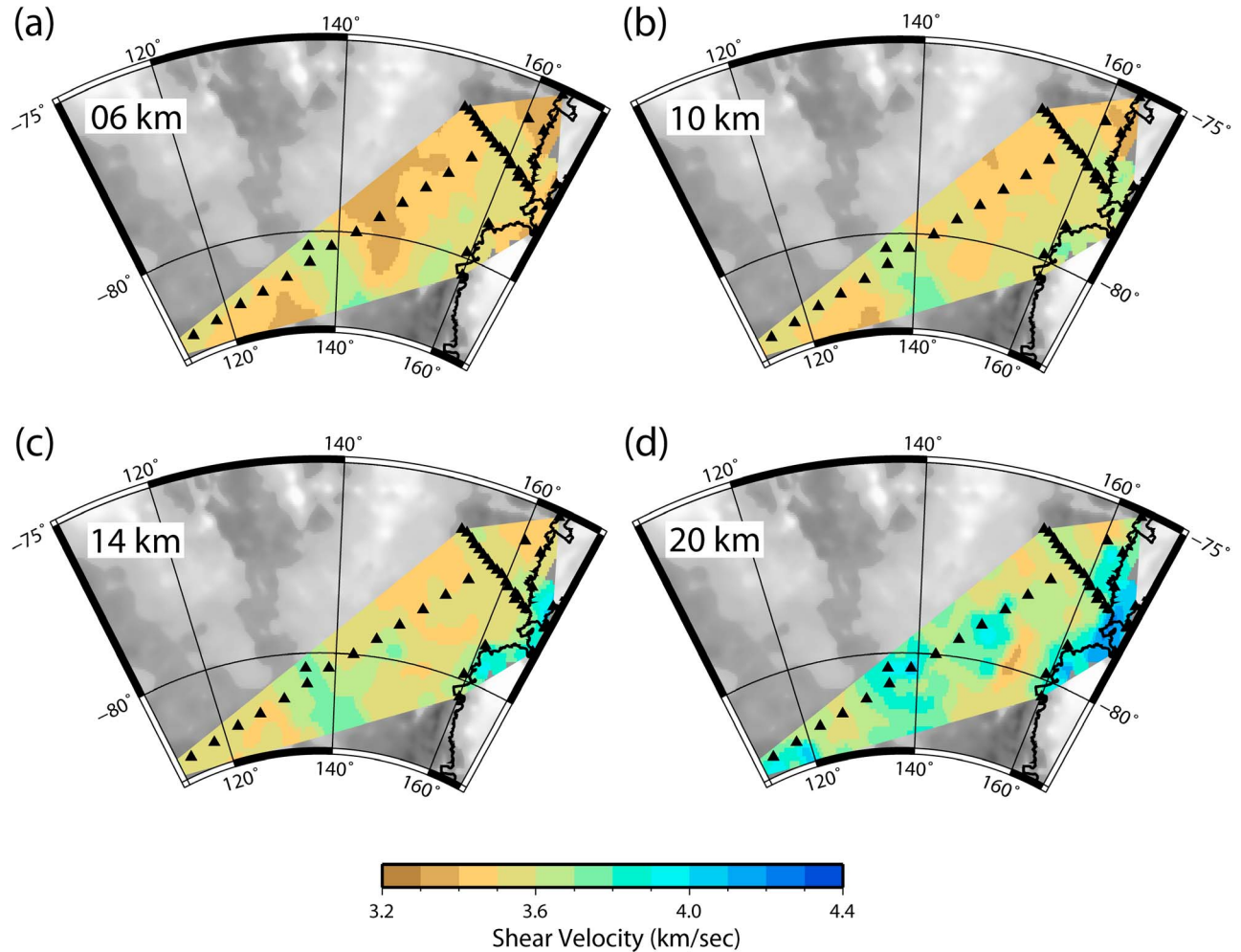


Figure 10. Shear velocity maps at depths of (a) 6, (b) 10, (c) 14, and (d) 20 km. Maps are constructed from the inversion of group velocity maps shown in Figure 6.

ties from our study at 20–23 s and the Lawrence *et al.* [2006b] study at 16 s in the RS region.

[23] Shear velocities in the RS appear to be about 3.2–3.3 km/s in the upper 10 km of the crust. Low velocities are expected at these depths based on results from several active source surveys which find up to 12 km of sedimentary rock or sedimentary rock mixed with volcanic flows [e.g., Behrendt *et al.*, 1991; Cooper *et al.*, 1987; Kim *et al.*, 1986]. Receiver function work at station SBA on Ross Island by Bannister *et al.* [2003] found shear velocities which increase from 2.0 to 3.7 km/s at these depths. Sediment velocities at shallow depths would certainly have lower velocities than the 3.2 km/s we observe; however, our data is less sensitive to the upper few kilometers, and the smoothing constraint placed on the shear velocity inversion may bias the shallowest velocities to higher values. Between 5 and 10 km, our results agree with the average seen by Bannister *et al.* [2003]. At 18 km depth our shear velocity maps begin to show upper mantle velocities beneath the RS of ~4.3 km/s, similar to the results of Lawrence *et al.* [2006b]. By 20–22 km depth, these high velocities are widespread beneath the RS. This agrees well with previous studies which have found Moho depths in the RS between 17 and 24 km [e.g., Behrendt, 1999; Behrendt

et al., 1991; Lawrence *et al.*, 2006a; O'Connell and Stepp, 1993; ten Brink *et al.*, 1993].

4.2. The Transantarctic Mountains

[24] Group velocities beneath the TAMs at short periods are up to 9%–12% higher than average, likely due to the lack of the ice layer covering EA and the thick sedimentation expected in the RS. The TAMs exhibit shear velocities which are ~3% higher than average for the region below depths of about 10 km. At the GSN station VNDA, located in the TAMs, Bannister *et al.* [2003] found velocities of 2.5–3.2 km/s for depths shallower than 10–12 km and 3.4–3.8 km/s for the midcrust. As for the RS, our results show higher velocities (~3.4 km/s) at shallow depths but agree deeper with velocities of 3.5–3.8 km/s at depths between 10 and 40 km. Other stations located in the TAMs for the Bannister *et al.* [2003] study found velocities closer to ours in the upper 10 km ranging from 3.0 to 3.4 km/s. Beyond depths of about 20–22 km our results do not show an increase in shear velocity associated with the Moho, but our peak sensitivity is to depths below 25 km and crustal thicknesses are expected to be between 38 and 40 km

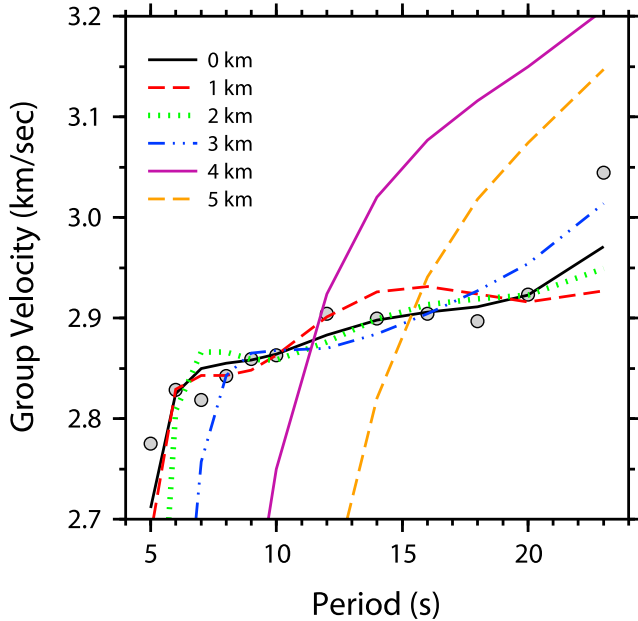


Figure 11. Inversion results from a node in the Wilkes Subglacial Basin with varying sediment layer thicknesses fixed. Gray circles represent observed group velocities where the line of seismic stations crosses the Wilkes Basin. Black solid line represents the predicted group velocities from the lowest cost shear velocity model from an inversion with no sediment required. Colored lines show the predicted dispersion curves of the best fitting structure with 1.0 km (dashed gray or red), 2.0 km (dotted light gray or green), 3.0 km (dash dotted dark gray or blue), 4.0 km (solid gray or purple), and 5.0 km (dashed dark gray or orange) of sediment imposed on the solution, respectively.

beneath the TAMs [e.g., *Della Vedova et al.*, 1997; *Lawrence et al.*, 2006a].

4.3. East Antarctica

[25] Very little information about the crustal structure of EA exists from previous studies. Geophysical studies have suggested the crustal thickness to be about 40–45 km [*Hansen et al.*, 2009], which is deeper than the peak sensitivity of our data. Our shear velocities show only minor changes at all depths beneath EA, suggesting that there is little variation with depth in the crust. The highest velocities are seen beneath the Belagica Highlands and are likely related to exposure of crystalline basement rocks near the surface. A similar interpretation was reached for high velocities obtained from noise correlation beneath mountain ranges in the western United States [*Moschetti et al.*, 2007]. Shear velocities at shallow depths beneath the Wilkes Subglacial Basin are lower than average. The basin is a long wavelength topographic depression which parallels the TAMs on the inland side. The origin of the basin is under some debate [e.g., *Drewry*, 1976; *Stern and ten Brink*, 1989; *Studinger et al.*, 2004], as is the amount of sediment infill which may be present. Results from *Drewry* [1976] and *Lawrence et al.* [2006a] suggest that there may be several kilometers of sediment within the basin, while studies by *Studinger et al.* [2004] and *ten Brink et al.* [1997] suggest

that there is no more than 1 km of sediment present. We observe velocities of ~3.2–3.3 km/s extending to around 8–10 km depth. Similar velocities appear in the vicinity of the Aurora Subglacial Basin where *Lawrence et al.* [2006a] also found a sedimentary layer to be required, although near this area our resolution begins to degrade due to lack of crossing raypaths. The velocities in these basins are lower than would be typical for upper crust of Precambrian age [*Bassin et al.*, 2000], which is the expected structure for East Antarctica [e.g., *Dalziel*, 1992]; however, they are higher than what might be expected for sediment.

[26] To investigate the possibility that the low observed upper crustal velocities may result from a sediment layer that is not well localized in depth, we reinvert the regional EA group velocity curve as well as velocity curves for several individual nodes within the Wilkes Basin with sediment layers of varying thickness required. In the new inversions, the ice layer is fixed with the same thicknesses described above (2 km for the regional EA and SOAR or BEDMAP thicknesses for individual nodes) and a sediment layer is also given a fixed thickness for six different runs of 0.0, 1.0, 2.0, 3.0, 4.0, and 5.0 km. Velocities for the sediment layer were estimated using sediment velocities from CRUST 2.0 [*Bassin et al.*, 2000]. Fits from these inversions to the group velocity curves for one Wilkes Basin node are shown in Figure 11. In all cases, model costs and misfits to the data increase with increasing sediment layer thickness. Inversions with 0–2 km of sediment may be considered to fit the data reasonably well, but sediment layers thicker than 2 km produce more significant misfits to the data. Models with 1–2 km of sediment included have velocities beneath the sediment that layer reach typical Precambrian upper crust values. These results suggest that low velocities in the region of the Wilkes Basin may indicate the presence of sediment, but the amount is likely less than a couple of kilometers.

5. Conclusions

[27] We utilize the cross correlation of ambient seismic noise recorded by the TAMSEIS array to obtain estimated Green's functions and examine Rayleigh waves at short periods for the Transantarctic Mountains and surrounding areas in the Ross Sea and East Antarctica. After performing a tomographic inversion for group velocity maps we obtain the best fitting average and regional shear velocity models and shear velocity maps from a niching genetic algorithm. We observe low shear velocities beneath the Ross Sea between 0 and 10 km depth and high velocities probably associated with the transition from crust to mantle between 16 and 20 km depth. Shear velocities beneath the Transantarctic Mountains and East Antarctica do not exhibit large variations suggesting there is little change in the seismic velocity of the crust. We observe low velocities of 3.2–3.3 km/s beneath the Wilkes Subglacial Basin, which may represent a small amount of sediment but suggests that there is not a thick sediment layer within the basin in our study area.

[28] **Acknowledgments.** We thank Mitchell Barklage, Bruce Beaudoin, Maggie Benoit, James Condor, Audrey Huerta, Jesse Lawrence, Bob Osborn, Tim Parker, Sara Pozgay, Brian Shiro, Patrick Shore, Rigobert Tibi, Don Voigt, Tim Watson, and many others for their assistance in the

deployment and collection of seismic instruments. We also thank two anonymous reviews for helpful suggestions on the manuscript. Portable seismic instrumentation for this project was obtained from the PASSCAL program of the Incorporated Research Institutions in Seismology (IRIS), and data handling assistance was provided by the IRIS Data Management System. This research was conducted with support from NSF grants OPP9909603 and OPP9909648.

References

- Anandakrishnan, S., and J. P. Winberry (2004), Antarctic subglacial sedimentary layer thickness from receiver function analysis, *Global Planet. Change*, **42**, 167–176.
- Anandakrishnan, S., D. D. Blankenship, R. B. Alley, and P. L. Stoffa (1998), Influence of subglacial geology on the position of a West Antarctic ice stream from seismic observations, *Nature*, **394**, 62–65.
- Bannister, S., J. Yu, B. Leitner, and B. L. N. Kennett (2003), Variations in crustal structure across the transition from West to East Antarctica, southern Victoria Land, *Geophys. J. Int.*, **155**, 870–884.
- Barmin, M. P., M. H. Ritzwoller, and A. L. Levshin (2001), A fast and reliable method for surface wave tomography, *Pure Appl. Geophys.*, **158**, 1351–1375.
- Bassin, C., G. Laske, and G. Masters (2000), The current limits of resolution for surface wave tomography in North America, *Eos Trans. AGU*, **81** (48), Fall Meet. Suppl., Abstract S12A-03.
- Behrendt, J. C. (1999), Crustal and lithospheric structure of the West Antarctic Rift System from geophysical investigations – a review, *Global Planet. Change*, **23**, 25–44.
- Behrendt, J. C., W. E. LeMasurier, A. K. Cooper, F. Tessensohn, A. Treku, and D. Damaske (1991), Geophysical studies of the West Antarctic Rift System, *Tectonics*, **10**, 1257–1273.
- Bell, R. E., D. D. Blankenship, C. A. Finn, D. L. Morse, T. A. Scambos, J. M. Brozena, and S. M. Hodge (1998), Influence of subglacial geography on the onset of a West Antarctic ice stream from aerogeophysical observations, *Nature*, **394**, 58–62.
- Bensen, G. D., M. H. Ritzwoller, M. P. Barmin, A. L. Levshin, F.-C. Lin, M. P. Moschetti, N. M. Shapiro, and Y. Yang (2007), Processing seismic ambient noise data to obtain reliable broad-band surface wave dispersion measurements, *Geophys. J. Int.*, **169**, 1239–1260.
- Bensen, G. D., M. H. Ritzwoller, and N. M. Shapiro (2008), Broadband ambient noise surface wave tomography across the United States, *J. Geophys. Res.*, **113**, B05306, doi:10.1029/2007JB005248.
- Bentley, C. R. (1991), Configuration and structure of the subglacial crust, in *The Geology of Antarctica*, edited by R. J. Tingey, pp. 335–364, Oxford Univ. Press, Oxford, UK.
- Blankenship, D. D., D. L. Morse, C. A. Finn, R. E. Bell, M. E. Peters, S. D. Kempf, S. M. Hodge, M. Studinger, J. C. Behrendt, and J. M. Brozena (2001), Geologic controls on the initiation of rapid basal motion for West Antarctic ice streams: A geophysical perspective including new airborne radar sounding and laser altimetry results, in *The West Antarctic Ice Sheet: Behavior and Environment*, edited by R. B. Alley and R. A. Bindschadler, pp. 105–121, AGU, Washington, D. C.
- Campillo, M., and A. Paul (2003), Long-range correlations in the diffuse seismic coda, *Science*, **299**, 547–549.
- Cooper, A. K., F. J. Davey, and J. C. Behrendt (1987), Seismic stratigraphy and structure of the Victoria Land Basin, western Ross Sea, Antarctica, in *The Antarctic Continental Margin: Geology and Geophysics of the Western Ross Sea*, edited by A. K. Cooper and F. J. Davey, pp. 27–76, Circum-Pacific Council for Energy and Mineral Resources, Houston, TX.
- Dalziel, I. W. D. (1992), Antarctica: A tale of two supercontinents?, *Annu. Rev. Earth Planet. Sci.*, **20**, 501–526.
- Danesi, S., and A. Morelli (2001), Structure of the upper mantle under the Antarctic Plate from surface wave tomography, *Geophys. Res. Lett.*, **28**, 4395–4398.
- DeConto, R. M., and D. Pollard (2003), Rapid Cenozoic glaciation of Antarctica induced by declining atmospheric CO₂, *Nature*, **421**, 245–249.
- Della Vedova, B., G. Pellis, H. Trey, J. Zhang, A. K. Cooper, J. Makris, and the ACRUP Working Group (1997), Crustal structure of the Transantarctic Mountains, Western Ross Sea, in *The Antarctic Region: Geological Evolution and Processes; Proceedings of the VII International Symposium on Antarctic Earth Sciences*, edited by C. A. Ricci, pp. 609–618, Terra Antarctica Publ., Sienna, Italy.
- Derode, A., E. Larose, M. Tanter, J. D. Rosny, A. Tourin, M. Campillo, and M. Fink (2003), Recovering the Green's function from field-field correlations in an open scattering medium, *J. Acoust. Soc. Am.*, **113**(6), 2973–2976.
- Donda, F., G. Brancolini, P. E. O'Brien, L. De Santis, and C. Escutia (2007), Sedimentary processes in the Wilkes Land margin: A record of the Cenozoic East Antarctic Ice Sheet evolution, *J. Geol. Soc. Am.*, **164**, 243–256.
- Drewry, D. J. (1976), Sedimentary basins of the East Antarctic Craton from geophysical evidence, *Tectonophysics*, **36**, 301–314.
- Dziewonski, A., S. Bloch, and M. Landisman (1969), A technique for the analysis of transient seismic signals, *Bull. Seismol. Soc. Am.*, **59**, 427–444.
- Dziewonski, A. M., and D. L. Anderson (1981), Preliminary reference Earth model, *Phys. Earth Planet. Inter.*, **25**, 297–356.
- Efron, B., and R. Tibshirani (1991), Statistical data analysis in the computer age, *Science*, **253**, 390–395.
- Escutia, C., L. De Santis, F. Donda, R. B. Dunbar, A. K. Cooper, G. Brancolini, and S. L. Eittreim (2005), Cenozoic ice sheet history from East Antarctic Wilkes land continental margin sediments, *Global Planet. Change*, **45**, 51–81.
- Hansen, S. E., J. Julia, A. A. Nyblade, M. L. Pyle, D. A. Wiens, and S. Anandakrishnan (2009), Using S-wave receiver functions to estimate crustal structure beneath ice sheets: An application to the Transantarctic Mountains and East Antarctic Craton, *Geochem. Geophys. Geosyst.*, **10**, Q08014, doi:10.1029/2009GC002579.
- Herrmann, R. B. (1978), *Computer Programs in Earthquake Seismology*, vol. 2, *Surface Wave Programs*, Dept. of Earth and Atmospheric Sciences, St. Louis Univ., St. Louis, Missouri.
- Holt, J. W. (2001), Airborne surveys conducted by SOAR for geologic studies in Antarctica, 1998–2001, *Eos Trans. AGU*, **82**, Spring Meet. Suppl., Abstract GP42A-07.
- Kanao, M., A. Kubo, T. Shibutani, H. Negishi, and Y. Tono (2002), Crustal structure around the Antarctic margin by teleseismic receiver function analyses, in *Antarctica at the Close of a Millennium; Proceedings of the 8th International Symposium on Antarctic Earth Sciences*, edited by J. A. Gamble et al., Royal Society of New Zealand, Wellington, New Zealand.
- Kim, Y., L. D. McGinnis, and R. H. Bowen (1986), The Victoria Land Basin: Part of an extended crustal complex between East and West Antarctica, in *Reflection Seismology: The Continental Crust*, edited by M. Barazangi and L. D. Brown, pp. 323–330, AGU, Washington, D. C.
- Koper, K. D., M. E. Wysession, and D. A. Wiens (1999), Multimodal function optimization with a niching genetic algorithm: A seismological example, *Bull. Seismol. Soc. Am.*, **89**, 978–988.
- Lawrence, J. F., and D. A. Wiens (2004), Combined receiver-function and surface wave phase-velocity inversion using a niching genetic algorithm: Application to Patagonia, *Bull. Seismol. Soc. Am.*, **94**, 977–987.
- Lawrence, J. F., D. A. Wiens, A. A. Nyblade, S. Anandakrishnan, P. J. Shore, and D. Voigt (2006a), Crust and upper mantle structure of the Transantarctic Mountains and surrounding regions from receiver functions, surface waves, and gravity: Implications for uplift models, *Geochem. Geophys. Geosyst.*, **7**, Q10011, doi:10.1029/2006GC001282.
- Lawrence, J. F., D. A. Wiens, A. A. Nyblade, S. Anandakrishnan, P. J. Shore, and D. Voigt (2006b), Rayleigh wave phase velocity analysis of the Ross Sea, Transantarctic Mountains and East Antarctica from a temporary seismograph array, *J. Geophys. Res.*, **111**, B06302, doi:10.1029/2005JB003812.
- Lin, F.-C., M. H. Ritzwoller, J. Townend, S. Bannister, and M. K. Savage (2007), Ambient noise Rayleigh wave tomography of New Zealand, *Geophys. J. Int.*, **170**, 649–666.
- Lobkis, O. I., and R. L. Weaver (2001), On the emergence of the Green's function in the correlations of a diffuse field, *J. Acoust. Soc. Am.*, **110**(6), 3011–3017.
- Lythe, M. B., D. G. Vaughan, and the BEDMAP Consortium (2001), BEDMAP: A new ice thickness and subglacial topographic model of Antarctica, *J. Geophys. Res.*, **106**, 11,335–11,351.
- Mafoud, S. W. (1995), Niching methods for genetic algorithms, Ph.D. thesis, Univ. of Illinois, Urbana-Champaign.
- Morelli, A., and S. Danesi (2004), Seismological imaging of the Antarctic continental lithosphere: A review, *Global Planet. Change*, **42**, 155–165.
- Moschetti, M. P., M. H. Ritzwoller, and N. M. Shapiro (2007), Surface wave tomography of the western United States from ambient seismic noise: Rayleigh wave group velocity maps, *Geochem. Geophys. Geosyst.*, **8**, Q08010, doi:10.1029/2007GC001655.
- O'Connell, D. R. H., and T. M. Stepp (1993), Structure and evolution of the crust at the Transantarctic Mountains–Ross Sea crustal transition: Results from the Tourmaline Plateau seismic array of the GANOVEX V ship-to-shore seismic refraction experiment, *Geol. J.*, **47**, 229–276.
- Paul, A., M. Campillo, L. Margerin, E. Larose, and A. Derode (2005), Empirical synthesis of time-asymmetrical Green functions from the correlation of coda waves, *J. Geophys. Res.*, **110**, B08302, doi:10.1029/2004JB003521.
- Ravat, D., Z. Lu, and L. W. Braile (1999), Velocity-density relationships and modeling the lithospheric density variations of the Kenya Rift, *Tectonophysics*, **302**, 225–240.

- Ritzwoller, M. H., N. M. Shapiro, A. L. Levshin, and G. M. Leahy (2001), Crustal and upper mantle structure beneath Antarctica and surrounding oceans, *J. Geophys. Res.*, **106**, 30,645–30,670.
- Roult, G., D. Rouland, and J. P. Montagner (1994), Antarctica II: Upper-mantle structure from velocities and anisotropy, *Phys. Earth Planet. Inter.*, **4**, 33–57.
- Sabra, K. G., P. Gerstoft, P. Roux, W. A. Kuperman, and M. C. Fehler (2005a), Extracting time-domain Green's function estimates from ambient seismic noise, *Geophys. Res. Lett.*, **32**, L03310, doi:10.1029/2004GL021862.
- Sabra, K. G., P. Gerstoft, P. Roux, W. A. Kuperman, and M. C. Fehler (2005b), Surface wave tomography from microseisms in Southern California, *Geophys. Res. Lett.*, **32**, L14311, doi:10.1029/2005GL023155.
- Shapiro, N. M., and M. Campillo (2004), Emergence of broadband Rayleigh waves from correlations of the ambient seismic noise, *Geophys. Res. Lett.*, **31**, L07614, doi:10.1029/2004GL019491.
- Shapiro, N. M., M. Campillo, L. Stehly, and M. H. Ritzwoller (2005), High-resolution surface wave tomography from ambient seismic noise, *Science*, **307**, 1615–1618.
- Stern, T. A., and U. S. ten Brink (1989), Flexural uplift of the Transantarctic Mountains, *J. Geophys. Res.*, **94**, 10,315–10,330.
- Studinger, M., R. E. Bell, W. R. Buck, G. D. Karner, and D. D. Blankenship (2004), Sub-ice geology inland of the Transantarctic Mountains in light of new aerogeophysical data, *Earth Planet. Sci. Lett.*, **220**, 391–408.
- ten Brink, U. S., S. Bannister, B. C. Beaudoin, and T. A. Stern (1993), Geophysical investigations of the tectonic boundary between East and West Antarctica, *Science*, **261**, 45–50.
- ten Brink, U. S., R. I. Hackney, S. Bannister, T. A. Stern, and Y. Makovsky (1997), Uplift of the Transantarctic Mountains and the bedrock beneath the East Antarctic ice sheet, *J. Geophys. Res.*, **102**, 27,603–27,621.
- Watson, T., A. A. Nyblade, D. A. Wiens, S. Anandakrishnan, M. Benoit, P. J. Shore, D. Voigt, and J. VanDecar (2006), P and S velocity structure of the upper mantle beneath the Transantarctic Mountains, East Antarctic craton, and Ross Sea from travel time tomography, *Geochem. Geophys. Geosyst.*, **7**, Q07005, doi:10.1029/2005GC001238.
- Yang, Y., M. H. Ritzwoller, A. L. Levshin, and N. M. Shapiro (2007), Ambient noise Rayleigh wave tomography across Europe, *Geophys. J. Int.*, **168**, 259–274.
-
- S. Anandakrishnan and A. A. Nyblade, Department of Geosciences, Pennsylvania State University, University Park, PA 16802, USA.
 M. L. Pyle, Department of Geology and Geophysics, University of Utah, Salt Lake City, UT 84112, USA. (mpyle@wustl.edu)
 D. A. Wiens, Department of Earth and Planetary Sciences, Washington University in St. Louis, St. Louis, MO 63130, USA.